Princeton Plasma Physics Laboratory

PPPL- 4989

PPPL- 4989

The Effects of Finite Electron Temperature and Diffraction on Lower Hybrid Wave Propagation

J.C. Wright and N. Bertelli

FEBRUARY, 2014

Prepared for the U.S. Department of Energy under Contract DE-AC02-09CH11466.

Princeton Plasma Physics Laboratory
Report Disclaimers

Full Legal Disclaimer

Trademark Disclaimer

PPPL Report Availability

Princeton Plasma Physics Laboratory:

http://www.pppl.gov/techreports.cfm

Office of Scientific and Technical Information (OSTI):

http://www.osti.gov/bridge

Related Links:

U.S. Department of Energy

Office of Scientific and Technical Information

Fusion Links

IOP Publishing Plasma Physics and Controlled Fusion
Plasma Phys. Control. Fusion **56** (2014) 035006 (7pp) doi:10.1088/0741-3335/56/3/035006

The effects of finite electron temperature and diffraction on lower hybrid wave propagation

J C Wright[1] **and N Bertelli**[2]

[1] Plasma Science and Fusion Center, Massachusetts Institute of Technology, Cambridge, MA 02139, USA
[2] Princeton Plasma Physics Laboratory, Princeton, NJ 08543, USA

E-mail: jcwright@mit.edu

Received 4 October 2013, revised 24 December 2013
Accepted for publication 10 January 2014
Published 5 February 2014

Abstract

In this paper we show that the commonly used cold plasma dispersion relation for plasma waves in the lower hybrid range of frequencies (LHRF) produces a wave trajectory that is notably different than when thermal corrections to the Hermitian part of the dielectric tensor are retained. This is in contrast to the common implementation in LH simulation codes in which thermal effects are retained only for the anti-Hermitian part of the dielectric tensor used for damping calculations. We show which term is the critical one to retain in the dielectric tensor and discuss implications for modeling of LHRF waves in present day and future devices. We conclude with some observations on the effects of diffraction that may be isolated once thermal effects are retained in both ray tracing and full-wave approaches.

Keywords: lowerhybrid, diffraction, fullwave, ray tracing

(Some figures may appear in colour only in the online journal)

1. Introduction

In theory and modeling of lower hybrid (LH) waves it is conventional to use the cold plasma model for propagation and only to invoke finite electron temperature effects in electron Landau damping [1, 2]. The original proposed purpose of LH waves was as a method of heating ions through mode conversion to the ion plasma wave from the slow wave at the LH resonance [3, 4] . This scenario permitted the neglection of the contribution of terms lower order in the perpendicular wave number. That is, the leading order $n_\perp^6$ term introduced by the inclusion of finite Larmor radius effects together with the assumption that $n_\perp \gg n_\parallel$ near the LH resonance discouraged the investigation of thermal corrections to the terms $\mathcal{O}^2$ and $\mathcal{O}^0$ in $n_\perp$. We shall show that the assumptions in this physical situation do not apply to the use of the cold plasma dispersion relation to describe LH ray trajectories in current drive scenarios and can miss important thermal corrections when the LH ray is launched directly.

LH waves have been simulated using geometric optics (ray tracing) [5–9], paraxial Wentzel–Kramers–Brillouin (pWKB) approximation (beam tracing) [10, 11], hybrid WKB/full wave [12] and physical optics (full wave) [13–17]. Discrepancies between the results of these approaches have been attributed to diffraction and focusing. We shall show that while these effects remain in comparisons between ray tracing and beam tracing/full wave, primarily there can also be significant differences due to different dispersion relation models in those codes.

In the first part of this paper, we will show that full kinetic effects of finite temperature electrons must be retained in the parallel contributions to the dielectric tensor to obtain accurate propagation as well as damping. Counter-intuitively, the thermal corrections are not important for the high temperature ($T_e > 10$ keV) fusion reactor plasmas due to the short propagation path limited by strong absorption. The effect is observed if a given family of rays are sufficiently weakly damped that they encircle the magnetic axis and so are in the 'multipass' regime. We will quantify this effect for some simple cases and show that it is present for the parameters of present day tokamaks.

Identifying the importance of kinetic effects in LH propagation permits a careful and controlled comparison

between ray tracing and full wave using the same dielectric properties. The use of ray tracing to determine trajectories relies on a small wavelength compared to system scale lengths and is accurate in determining the direction of energy propagation until focusing and thus diffraction begins to play a role [11]. In the second part of this paper, we show that the flux averaged power densities are reduced relative to ray tracing when full-wave effects are taken into account.

2. Background

LH waves were proposed [3] for ion heating through mode conversion to ion plasma waves at the LH resonance, $\omega = \omega_{\rm lh}$ where

$$\omega_{\rm lh} \equiv \left[(\Omega_{\rm ce}\Omega_{\rm ci})^{-1} + \omega_{\rm pi}^{-2}\right]^{-1/2} \approx \sqrt{\Omega_{\rm ce}\Omega_{\rm ci}}$$

is the LH frequency.

Thermal effects were believed to a play a role in propagation only through the finite values of electron and ion temperatures near resonance and in damping through $\zeta \equiv (\omega/k_\parallel)/v_{\rm te}$ in Landau damping and not in parallel dispersion. Here the perpendicular and parallel wave numbers are $k_\perp$ and $k_\parallel$, $v_{\rm te} = \sqrt{2T_{\rm e}/m_{\rm e}}$ is the electron thermal velocity and ω is the wave frequency. Hence, ζ is the ratio of the wave parallel phase velocity to the electron thermal speed. At the LH resonance, the leading coefficient in the fourth order (in perpendicular index of refraction, $n_\perp$) cold plasma LH dispersion vanishes and the equation is singular in $n_\perp$ there. In the limit of large $n_\perp$ where $n_\perp \gg n_\parallel$, the wave is primarily electrostatic. The leading order correction from the retention of finite electron and ion temperature effects raises the order of the equation to $n_\perp^6$ [18, 19].

The resultant warm plasma LH dispersion relation,

$$P_6 n_\perp^6 + P_4 n_\perp^4 + P_2 n_\perp^2 + P_0 = 0, \tag{1}$$

describes a slow and a fast wave and the ion plasma wave. The parallel and perpendicular indices of refraction are given by $n_{\parallel,\perp} = k_{\parallel,\perp}\omega/c$. In magnetically confined fusion plasmas where magnetic fields are on the order of several Tesla, $\omega_{\rm lh}$ will be on the order of several gigahertz. The coefficients are defined in terms of the Stix [4] cold plasma dielectric tensor elements:

$$P_6 = -3\left(\frac{\omega_{\rm pi}}{\omega}\frac{v_{\rm ti}}{c}\right)^2 - (3/4)\left(\frac{\omega}{\Omega_{\rm ce}}\frac{\omega_{\rm pe}}{\Omega_{\rm ce}}\frac{v_{\rm te}}{c}\right)^2, \tag{2}$$

$$P_4 = S,$$

$$P_2 = (S+P)(n_\parallel^2 - S) + D^2,$$

$$P_0 = P\left[(n_\parallel^2 - S)^2 - D^2\right],$$

as given in [9, 18, 20, 21]. Near the LH resonance where $S \to 0$ and mode conversion occurs, this correction resolves the resulting singularity by introducing a higher order term, $n_\perp^6$ that is proportional to the electron temperature through the plasma electron beta, $\beta_e = (\omega_{\rm pe}v_{\rm te}/\Omega_{\rm ce}c)^2$ and the ion temperature. Near the LH resonance, the $n_\perp^6$ term dominants the dispersion and thermal effects in the lower order terms may be neglected.

Modern usage of LH waves is for current drive and not ion heating. Therefore, LH is applied in the regime where $\omega > 2\omega_{\rm lh}$ to avoid edge parametric decay modes [22, 23] and ion interaction. The LH resonance is not in the plasma and so the thermal corrections just discussed are not included. Instead, the fourth order version of equation (1) is used with linear damping calculated separately from a hot plasma dispersion relation. Motivated by observed discrepancies in previous LHRF modeling benchmarks [10, 13], we have found significant differences in predicted trajectories of LH paths from ray tracing between the cold plasma model and the full hot plasma dielectric tensor.

3. Hot electron effects

When calculating the trajectories of LH waves, it has been commonly assumed that the paths are independent of electron temperature and the cold plasma dispersion relation may be used. In figure 1, we test this assumption by using the full hot dispersion relation including all cyclotron harmonics and thermal effects [4] in the GENRAY [8] code. We compare rays for a range of electron temperatures from 0.01 to 10 keV to the cold plasma prediction. The rays paths are plotted until all (>99%) of the power on that ray is absorbed. The hot plasma ray trajectories converge to the cold plasma ray trajectories as the electron temperature is lowered but large differences in the poloidal location of the first reflection remain even at temperatures as low as 0.5 keV. Differences in the trajectories do not appear until some poloidal propagation takes place. Hence we conclude that for temperatures approaching $T_{\rm e} = 10$ keV such as in the ITER device there is little difference from the cold plasma trajectory before absorption occurs.

To further isolate the source of this additional dispersion, we consider what terms are important in the LHRF. Because of the high frequency relative to the ion gyro-frequency the ion harmonic terms should not be important. Similarly, $\omega_{\rm lh}$ is far below the electron gyro-frequency and so the electron harmonics may be neglected. The largest Landau term is the Stix parallel component of the dielectric tensor, P, which is proportional to the electron and ion plasma frequencies. The electron term is dominant, so we consider the thermal corrections to the electrons and keep the ions cold. In equations (3*a*)–(3*c*), successive approximations to the parallel dielectric term, $P(\zeta)$, are given: the zeroth order for the cold plasma expression in equation (3*a*), to $\mathcal{O}(-2)$ in ζ (from $\mathcal{O}(-5)$ expansion of $Z(\zeta)$) in equation (3*b*) and $\mathcal{O}(-6)$ in ζ (from $\mathcal{O}(-9)$ expansion of $Z(\zeta)$) in equation (3*c*).

$$P = 1 - \frac{\omega_{\rm pe}^2}{\omega^2} - \frac{\omega_{\rm pi}^2}{\omega^2}, \tag{3a}$$

$$P = 1 - \frac{\omega_{\rm pe}^2}{\omega^2}\left(1 + \frac{3}{2}\frac{k_\parallel^2 v_{\rm th}^2}{\omega^2}\right) - \frac{\omega_{\rm pi}^2}{\omega^2}, \tag{3b}$$

$$P = 1 - \frac{\omega_{\rm pe}^2}{\omega^2}\left(1 + \frac{3}{2}\frac{k_\parallel^2 v_{\rm th}^2}{\omega^2} + \frac{15}{4}\frac{k_\parallel^4 v_{\rm th}^4}{\omega^4} + \frac{105}{8}\frac{k_\parallel^6 v_{\rm th}^6}{\omega^6}\right) - \frac{\omega_{\rm pi}^2}{\omega^2}, \tag{3c}$$

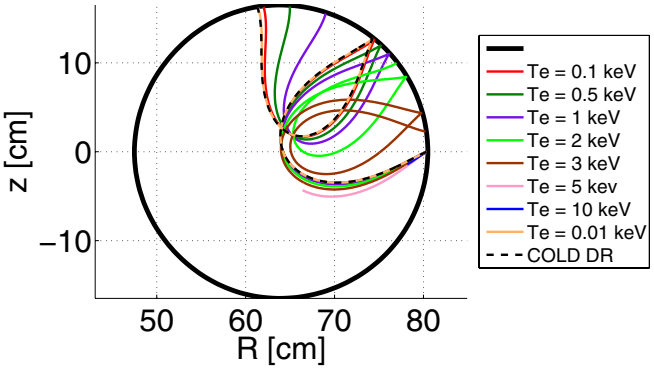

Figure 1. Ray trajectories using full hot plasma dispersion relation for various temperatures compared with ray from cold plasma dispersion relation. Rays end when 99% of power is absorbed. Plasma parameters are $n_e = 5 \times 10^{19}\,\mathrm{m}^{-3}$, $B_0 = 8\,\mathrm{T}$, $n_\parallel = -2.5$, $a = 16.5\,\mathrm{cm}$, $R_0 = 64.0\,\mathrm{cm}$, δ(Shafranov shift) $= -0.97\,\mathrm{cm}$. Density and temperature have parabolic profiles. Rays are launched at $R = 80.4\,\mathrm{cm}$ $Z = 0\,\mathrm{cm}$.

which are just terms in the asymptotic series expansion of the full kinetic expression involving the plasma dispersion function, $Z(\zeta)$:

$$P(\zeta) = 1 - \frac{\omega_{\mathrm{pe}}^2}{\omega^2}\zeta^2 Z'(\zeta) - \frac{\omega_{\mathrm{pi}}^2}{\omega^2}. \tag{4}$$

The parameter in the thermal correction, ζ, is the parallel wave phase velocity normalized to the electron thermal velocity and is typically a large number (∼4–7) such that perhaps equations (3*b*) or (3*c*) might be expected to be sufficient to capture the thermal effects. The correction from equation (3*b*) was retained in [21] along with the thermal corrections for the $n_\perp^6$ coefficient in equation (2), but in that study the authors emphasized that the $n_\perp^6$ term was the important thermal correction. But numerical tests using ray tracing show that after the first reflection even the sixth order (in ζ) correction in equation (3*c*) begins to noticeably depart from the full hot plasma dielectric tensor. The same numerical tests show that using the plasma dispersion function correction to the Landau term of $P(\zeta)$ as in equation (4) is sufficient to capture all the dispersion of waves in the LHRF from the full hot plasma dispersion relation. Figure 2 demonstrates this explicitly by showing rays for the same conditions calculated under successive corrections to the $P(\zeta)$ term. It is evident that the Z-function correction to $P(\zeta)$ produces a ray trajectory nearly identical to the one produced using the full hot plasma dielectric.

Additional poloidal dependence introduced in $P(\zeta)$ through the thermal correction leads to changes in $k_\parallel$ and z evolution. For simplicity, consider the cold plasma electrostatic dispersion relation, $\mathcal{D} = Sk_\perp^2 + Pk_\parallel^2 = 0$. The evolution of the parallel position, z, of the ray versus time, t, is given by $\partial z/\partial t = -(\partial\mathcal{D}/\partial k_\parallel)/(\partial\mathcal{D}/\partial\omega)$. We find

$$\frac{\partial\mathcal{D}}{\partial k_\parallel} = 2P(\zeta)k_\parallel - \frac{\omega}{v_{\mathrm{te}}}\frac{\partial P(\zeta)}{\partial\zeta}, \tag{5}$$

with second term being new. Both terms contain new dependence on the poloidal position through ζ that modifies the wave refraction. The new term provides an additional source for the change in the ray trajectory seen. There are additional contributions to evolution in the flux component, ψ, of the wave number due to the temperature dependence, $T_e(\psi)$, of ζ that have not been shown. Note that after substituting for ζ in $\partial P(\zeta)/\partial\zeta$, the leading order behavior of the new term is proportional to v_{te}^2 and so vanishes as $T_e \to 0$, as one would expect.

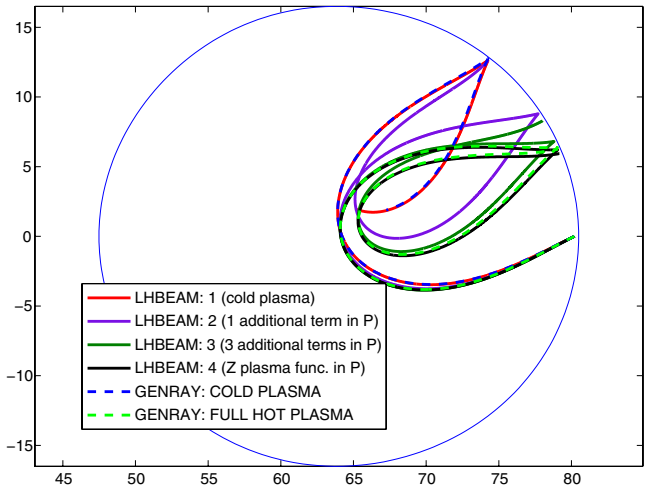

Figure 2. Rays with successive thermal corrections to the parallel dielectric term, $P(\zeta)$, are calculated by the LHBEAM code and are compared to calculations by GENRAY using the cold plasma dielectric and the full hot plasma dielectric. Both LHBEAM and GENRAY plots for the cold dielectric are shown as a simple benchmarking validation. Plasma and wave parameters are the same as those from figure 1.

3.1. Implementation in various codes

TORLH [16, 17] implements the kinetic form of $P(\zeta)$ in the LHRF limit as given in equation (4). It is a full-wave code that solves Maxwell's equations in the frequency domain using a mixed Fourier and finite element basis. The LHEAF code [13, 14] is a full-wave code using a finite element basis that implements a cold plasma approximation for $P(\zeta)$ as in equation (3*a*) and iteratively corrects the imaginary part of $P(\zeta)$ for damping but propagation is still determined by cold plasma dispersion. LHBEAM [10] uses the paraxial WKB approximation to solve for the wave fronts and beam propagation for the cold plasma dispersion relation and uses the linear electron Landau damping model for damping. The assumption of cold plasma dispersion for propagation is common enough that authors often do not describe the dielectric model in use in papers on LH waves. The cold plasma approximation is commonly used in ray tracing codes [5–7, 9]. Some codes, such as GENRAY [8] have options for cold and hot (kinetic) plasma dielectric models for LH but the cold dielectric tensor is still the primary model used by users[3] and in published benchmarks [7, 24].

3.2. Comparison of effects of rays for cold and hot plasma

In cases of strong absorption we have quantified the path differences. In this section, we quantify the effects on

[3] Personal communication with several users.

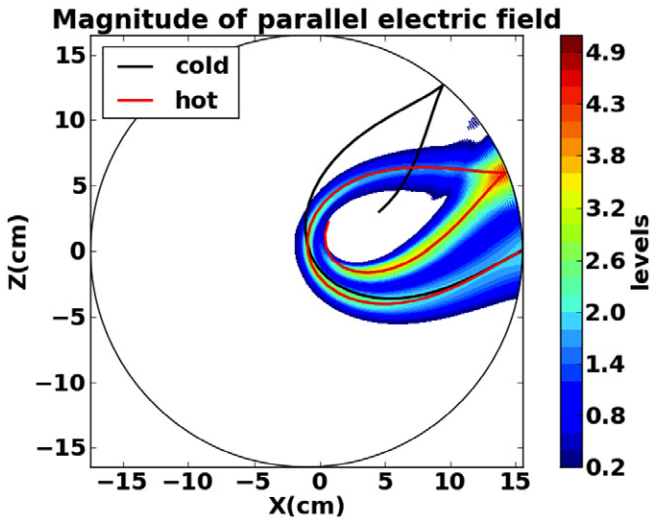

Figure 3. Ray trajectories with cold and hot plasma dielectrics from GENRAY are plotted over contours of the normalized magnitude of the parallel electric field from the full-wave solver TORLH. Parameters are $B_0 = 8\,\mathrm{T}$, $n_e = 5 \times 10^{19}\,\mathrm{m}^{-3}$, $n_\parallel = -2.5$ and $T_{e0} = 3\,\mathrm{keV}$. The electric field magnitude is normalized to the imposed field at the waveguide mouth. The minimum contour shown in the full-wave field plot is 5% of peak for clarity. Rays are launched at $X = 15.4\,\mathrm{cm}$ $Z = 0\,\mathrm{cm}$. The wave guide in the full-wave code is centered at the same location and has a height of 6.4 cm.

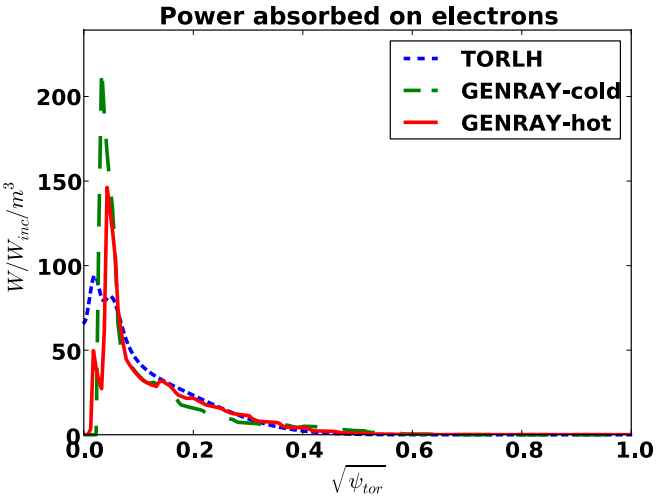

Figure 4. Flux averaged power for the solutions plotted in figure 3 using hot and cold dispersion relations in the GENRAY code and from the full-wave TORLH code. Normalized power densities are plotted as a function of the normalized square root of toroidal flux. Parameters are $B_0 = 8\,\mathrm{T}$, $n_e = 5 \times 10^{19}\,\mathrm{m}^{-3}$, $n_\parallel = -2.5$ and $T_{e0} = 3\,\mathrm{keV}$. X coordinate is centered on the magnetic axis.

LH deposited power density. The model circular plasma equilibrium used in figure 1 and through the examples in this paper is numerically generated equilibrium based on Alcator C parameters [25]. The parameters are also similar to the FTU tokamak [26]. Continuing with our model plasma equilibrium with a circular cross-section and central density of $n_e = 5 \times 10^{19}\,\mathrm{m}^{-3}$ and central magnetic field of $B_0 = 8\,\mathrm{T}$, we restrict the electron temperature to a single case of $T_{e0} = 3\,\mathrm{keV}$ and study the case of an LH wave with $n_\parallel = -2.5$ propagating under a hot and cold plasma dielectric.

In figure 3, we compare the computed ray paths employing cold and hot dielectrics to full-wave fields using a hot dielectric. In this case the hot dielectric for ray tracing is the full hot plasma kinetic dielectric and the hot dielectric for the full-wave code is the cold plasma LH dielectric with the modification of equation (4). We note that the hot dielectric ray follows the path of the electric field calculated in the full-wave code and even matches the length of the LH full-wave path. This demonstrates that the ray tracing path is consistent with the full-wave fields when both use a hot plasma dielectric. The agreement is further indication that the correction in equation (4) to $P(\zeta)$ is sufficient. The two different trajectories produced by hot and cold dielectric tensors also result in different power density deposition profiles.

In figure 4, the two power profiles from ray tracing and the one from full wave are compared. Despite the different trajectories, the two power deposition curves from ray tracing are similar. The power densities all agree well until the waves are within about a normalized minor radial coordinate, $\sqrt{\psi_{\mathrm{tor}}} \sim r/a$, of 0.1. The clearest difference is near the origin where we note the appearance of two peaks for the deposition from the hot plasma dielectric and one peak from the cold plasma dielectric. The power deposition curve from the full-wave code also has two peaks though they are wider. This is discussed further in section 4.1.

The difference in the power deposition seen in ray tracing with and without the finite electron temperature effect can be understood by referring to figure 5. In that figure, the ray from the cold plasma follows a trajectory that produces a higher upshift in $n_\parallel$ and results in damping of the ray before a second pass to the magnetic axis is complete. For the ray from the hot plasma, the $n_\parallel$ upshift is not as large and it reaches the axes a second time before damping. The different evolution rates of the parallel refractive index are caused indirectly by the different physical paths of the rays produced by the new term in equation (5). Reference [19] showed that the amount of upshift in the wave index is maximized near $\pm 90^\circ$, that is near the top and bottom of the cross-section of the plasma, and in figure 3 we indeed see that the cold ray trajectory is significantly closer to the 90° point than the warm ray.

In weak absorption regime the LH waves undergo many reflections and so one might expect the aggregate effect of finite electron temperature to be larger. The actual effect is that the rays become stochastic and space filling and trajectory differences have marginal effect on power deposition. Power deposition for both cases is broad. In a multipass scenario with $n_\parallel < 5.7/\sqrt{T_e}$ [27, 28] the LH waves are space filling. Thermal effects on the power deposition calculated with ray tracing show differences in peak locations but not in the width of the overall profile, figure 6. Because of the multiple reflections of rays, it is not possible to attribute physical effects to specific features as it was in the single pass case. In comparison with full wave, the power deposition from ray tracing is narrower even with both full wave and ray tracing using the same hot plasma dispersion relation. We attribute the differences from full wave in overall deposition broadness to diffraction and the resultant spectral broadening that is

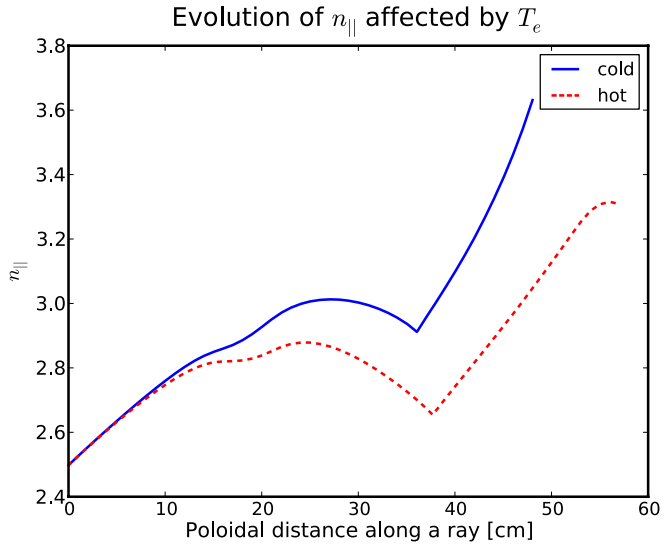

Figure 5. Evolution of the parallel index of refraction for hot and cold dispersion relations versus poloidal distance travelled by the ray for the same rays for which power is shown in figure 4 and the ray trajectories are shown in figure 3.

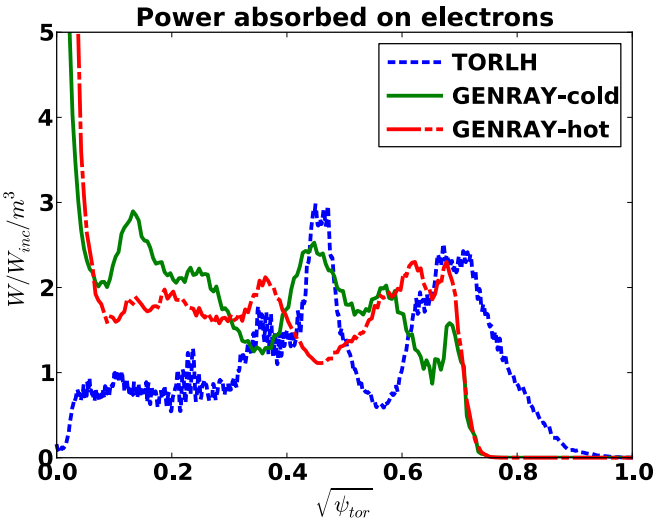

Figure 6. Finite electron temperature on power profile in multipass regime. Flux averaged power deposition from ray tracing and full-wave simulations are plotted as function of the square root of the normalized toroidal flux function, $\sqrt{\psi_{\rm tor}}$. In a multipass scenario with $n_{\|}\sqrt{T_{\rm e}} < 5.7$ the LH waves are space filling. Vertical axis was truncated from 25 to 5 to omit the high ray tracing on-axis power density and better show profile detail.

included in the full-wave model. This is discussed further in section 4.1 on diffraction effects.

In high density LH experiments in Alcator C-Mod [29], a sharp decline in hard x-ray emission and current drive has been observed. One candidate for this observed effect is the trajectory of the rays into the scrape-off region loosing power to collisional damping or parametric decay. This process is dependent on the path of the rays and therefore the finite electron temperature effect under discussion in this paper may play a role.

4. Diffraction effects

4.1. Focusing

In this comparison for the ray tracing results we use multiple launched rays covering the spatial extent of the launcher height to capture the finite width of the LH beam. Using a single ray produces flux averaged power density profiles that are narrower than full wave or beam tracing owing to the geometric projection of the LH beam power onto the flux surface [30] by averaging. A single ray does not account for finite beam width when the ray path is not normal to the flux surface. Using multiple rays that cover the spatial and spectral width of the launched waves captures the width of the beam. The ray bundle is shown in figure 7.

In a previous paper [10] the authors compared ray tracing and the paraxial beam approximation for the LH propagation in model equilibrium under discussion. We extend that comparison here with full-wave calculation that enables us to include reflections in the field calculations. We also employ a bundle of rays that have similar spectral and spatial widths to the antenna model in the full-wave code, TORLH. The poloidal width of the $n_{\|}$ spectrum from the full-wave code is used in the ray tracing code by having 8 rays launched with a separation in poloidal parallel index components covering the same spectral

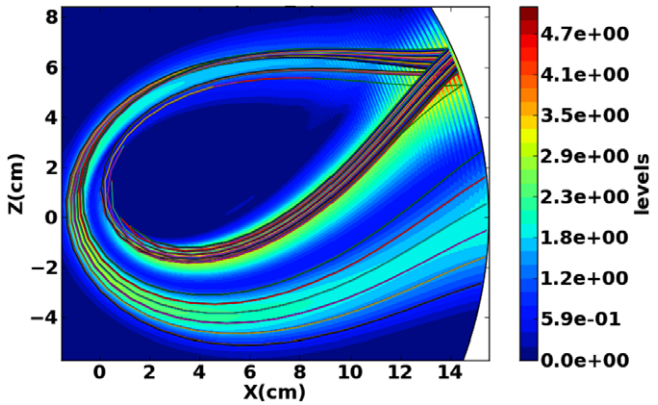

Figure 7. A ray bundle simulated using a finite electron temperature plasma dielectric. Same plasma parameters as in figure 4 but using 36 total rays with spectral separation equivalent to 1023 poloidal mode numbers and spatially spread across a 6.4 cm high waveguide. Rays are overlaid on contours of the magnitude of the normalized parallel electric field from the TORLH code. The full-wave simulation used 1000 radial cubic finite elements and 1023 poloidal modes.

width as in the full-wave antenna model. Similarly, multiple ray bundles are launched along the physical height of the antenna. In this way, we have very similar boundary/initial conditions used in both full wave and ray tracing.

In figure 7, we see that the ray paths overlaid on the full-wave contours of electric field magnitude follow each other closely until the waves turn near the magnetic axis (the origin in this plot.) At that point, the rays continue to focus while the full-wave fields reach a minimum beam width and actually begin to broaden again due to the effects of diffraction. Following the rays and beam further as they near the wall and reflect, the wave fields experience constructive and destructive interference, then reflect and make a second pass to the center where they both damp further creating the second peak seen in figure 8 at a normalized radius of 0.06.

4.2. Power deposition

After accounting for warm plasma effects we get much better overall agreement between the ray tracing and full-wave power deposition than in figure 8 of [10]. This permits this isolation of the diffraction effects. Referring to figure 8, we see that both models predict the double peaked aspect of the power resulting from the reflection. Accounting for the finite beam width results in a better match between power profiles outside of a normalized radius of 0.1 and also good agreement in the on-axis power density. The notable difference is the width and height of those two peaks. Recalling that the one-dimensional power deposition results from an average over the poloidal dimension, the consequence of focusing the power to a point in the toroidal cross-section as opposed to a finite spot size becomes evident. A finite width will spread the power across several flux surfaces whereas a point will always fall on just one surface. Thus ray tracing produces one-dimensional power deposition profiles that have narrower features and higher power densities than physical optics would predict. We note though, that this effect is minimized if the wave fronts are mostly parallel to the flux surfaces in the poloidal plane, that is propagation oblique to the flux surfaces. In this case there is no difference between a finite spot size and a point as far as the flux surface is concerned. This case arises primarily under strong single pass absorption where the wave does not penetrate to the center of the device, for example, in LH scenarios in the ITER device [14, 31].

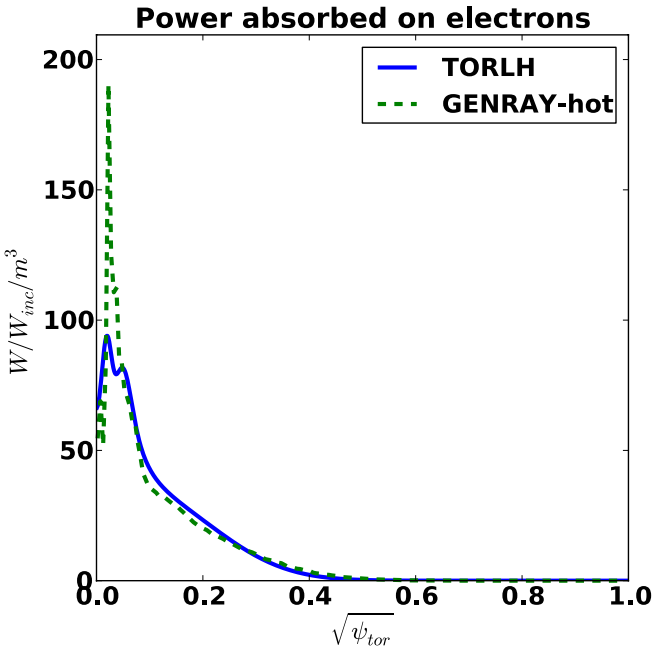

Figure 8. Flux averaged power deposition from ray tracing and full-wave simulations using a finite spatial and spectral spread of rays. The effects of diffraction near focal points inside a normalized flux radius of 0.1 produce broader peaks of deposition in full-wave results. Simulation parameters are the same as in figure 1. `GENRAY` ray tracing results are for a finite spread of 36 rays.

5. Conclusions

In this paper we have shown that the finite electron temperature has a significant effect on the propagation of lower hybrid (LH) waves and should be included in the real part of the dielectric tensor as well as the imaginary part. We further identified the relevant term as the Landau component of the parallel dielectric, $P(\zeta)$. The effect on flux averaged power is minor because of the exponential flux surface dependence of the electron Landau damping. However, the effect on propagation trajectory and wave number evolution is significant and could be important when other damping sources play a role; for example: collisional damping in the cold edge at high densities [32] and when the poloidal location of power deposition is a concern. It has also been shown recently [33] that nonlinear parametric decay processes can occur on the high field side (HFS) of the Alcator C-Mod device and may be responsible for the observed density limit in C-Mod. Analysis of these cases relies on accurate knowledge of the propagation path of the LH pump wave and thus the thermal effects on the ray trajectory paths discussed in this paper could be important in understanding the pump wave evolution.

Inclusion of this term in ray tracing, beam tracing, and full-wave codes is recommended especially in present day tokamaks with modest or weak damping ($n_\parallel\sqrt{T_e} < 5.7$). The ITER tokamak will operate at high electron temperatures ($T_{e0} > 15\,\mathrm{keV}$) with a parallel wave number, $n_\parallel = 2.5$ and will be in a strong single pass regime in which the LH waves will damp fully at approximately a normalized radius of 0.7. In this case, the short propagation distance with its poloidal component mainly normal to the flux surfaces does not produce significant differences between hot and cold plasma dispersion relations. Simulations not shown in this paper demonstrate that the power deposition location and shape is not changed to better than 1% and so for scenario development on ITER, the cold plasma model is sufficient. After accounting for electron thermal effects, a careful comparison between full wave and ray tracing was done to isolate diffraction effects. It was shown that the main effect was to limit focusing, modestly broaden the power deposition profile, and reduce the peak magnitude of the deposition relative to ray tracing.

Acknowledgments

We thank Paul Bonoli for helpful comments in the development of this paper. This work was supported by the SciDAC Center for Wave-Plasma Interactions Contract No DE-FC02-01ER54648 and US Department of Energy (DOE) Contract DE-AC02-CH0911466.

References

[1] Brambilla M 1976 *Plasma Phys.* **18** 699
[2] Cho S and Swanson D G 1988 *Phys. Fluids* **31** 1123–9
[3] Stix T H 1965 *Phys. Rev. Lett.* **15** 878–83
[4] Stix T H 1992 *Waves in Plasmas* (New York: American Institute of Physics)
[5] Heikkinen J A, Tala T J J, Pättikangas T J H, Piliya A D, Saveliev A N and Karttunen S J 1999 *Plasma Phys. Control. Fusion* **41** 1231
[6] Esterkin A R and Piliya A D 1996 *Nucl. Fusion* **36** 1501

[7] Peysson Y, Decker J and Morini L 2012 *Plasma Phys. Control. Fusion* **54** 045003
[8] Smirnov A P, Harvey R W and Kupfer K 1994 *Bull Am. Phys. Soc.* **39** 1626 (abstract 4R11)
[9] Imbeaux F and Peysson Y 2005 *Plasma Phys. Control. Fusion* **47** 2041
[10] Bertelli N, Maj O, Poli E, Harvey R, Wright J C, Bonoli P T, Phillips C K, Smirnov A P, Valeo E and Wilson J R 2012 *Phys. Plasmas* **19** 082510
[11] Pereverzev G V 1992 *Nucl. Fusion* **32** 1091–107
[12] Lu Z X, Zonca F and Cardinali A 2013 *Phys. Plasmas* **20** 032115
[13] Meneghini O, Shiraiwa S and Parker R 2009 *Phys. Plasmas* **16** 090701
[14] Shiraiwa S, Meneghini O, Parker R, Bonoli P, Garrett M, Wright J C and Wukitch S 2010 *Phys. Plasmas* **17** 056119
[15] Wright J C, Lee J, Valeo E, Bonoli P, Phillips C K, Jaeger E F and Harvey R W 2010 *IEEE Trans. on Plasma Sci.* **38** 2136–43
[16] Wright J C, Valeo E J, Phillips C K, Bonoli P T and Brambilla M 2008 *Commun. Comput. Phys.* **4** 545–55
[17] Wright J C, Bonoli P T, Schmidt A E, Phillips C K, Valeo E J, Harvey R W and Brambilla M A 2009 *Phys. Plasmas* **16** 072502
[18] Bonoli P 1984 *IEEE Trans. Plasma Sci.* **PS-12** 95–107
[19] Bonoli P T and Ott E 1982 *Phys. Fluids* **25** 359–75
[20] Brambilla M and Cardinali A 1982 *Plasma Phys.* **24** 1187–218
[21] Ignat D W 1981 *Phys. Fluids* **24** 1110–4
[22] Porkolab M 1977 *Phys. Fluids* **20** 2058–75
[23] Cesario R and Cardinali A 1989 *Nucl. Fusion* **29** 1709
[24] Bertelli N, Maj O, Poli E, Pereverzev G V, Peysson Y and Decker J 2008 *Theory of Fusion Plasmas: Joint Varenna-Lausanne International Workshop* (*AIP Conf. Proc.* vol 1069) ed O Sauter *et al* pp 259–64
[25] Porkolab M *et al* 1984 *Phys. Rev. Lett.* **53** 450–3
[26] Frigione D *et al* 1996 *Nucl. Fusion* **36** 1489
[27] Bonoli P T and Englade R C 1986 *Phys. Fluids* **29** 2937–50
[28] Brambilla M 1980 *Proc. Physics of Plasmas Close to ThermoNuclear Conditions* vol 17 (Brussels) p 291
[29] Wallace G M *et al* 2010 *Phys. Plasmas* **17** 082508
[30] Peysson Y and Decker J 2007 *17th Topical Conf. on Radio Frequency Power in Plasmas* 933 ed P Ryan and D Rasmussen (New York: American Institute of Physics) p 293
[31] Decker J *et al* 2011 *Nucl. Fusion* **51** 073025
[32] Wallace G M *et al* and the Alcator C-Mod Team 2011 *Nucl. Fusion* **51** 083032
[33] Baek S G, Parker R R, Shiraiwa S, Wallace G M, Bonoli P T, Brunner D, Faust I C, Hubbard A E, LaBombard B and Porkolab M 2013 *Plasma Phys. Control. Fusion* **55** 052001

The Princeton Plasma Physics Laboratory is operated
by Princeton University under contract
with the U.S. Department of Energy.

Information Services
Princeton Plasma Physics Laboratory
P.O. Box 451
Princeton, NJ 08543

Phone: 609-243-2245
Fax: 609-243-2751
e-mail: pppl_info@pppl.gov
Internet Address: http://www.pppl.gov